Inorg. Chem. **2004**, *43*, 8346–8354

Photochemical Expulsion of the Neutral Monodentate Ligand L in Ru(Terpy*)(Diimine)(L)$^{2+}$: A Dramatic Effect of the Steric Properties of the Spectator Diimine Ligand

Sylvestre Bonnet, Jean-Paul Collin,* Jean-Pierre Sauvage, and Emma Schofield†

Laboratoire de Chimie Organo-Minérale, UMR 7513 du CNRS, Université Louis Pasteur, Faculté de Chimie, 4, rue Blaise Pascal, 67070 Strasbourg Cedex, France

Received June 25, 2004

A series of photoreactive complexes of the type Ru(terpy*)(N–N)(L)$^{2+}$, where terpy* is 4′-(3,5-ditertiobutylphenyl)-2,2′:6′,2″-terpyridine, N–N is the bidentate chelate phen or dmp (phen = 1,10-phenanthroline, dmp = 2,9-dimethyl-1,10-phenanthroline), and L is the monodentate ligand dms, MeBN, or MeOBN (dms = dimethyl sulfide, MeBN = 2,6-dimethyl benzonitrile, MeOBN = 2,6-dimethoxybenzonitrile), has been synthesized and fully characterized by proton NMR spectroscopy, electrospray mass spectrometry, and UV–vis spectroscopy. The X-ray structures of four complexes were also obtained. In neat pyridine, the quantum yields for the photosubsitution of L by pyridine were measured and showed dramatic variations depending on the steric interactions between the spectator bidentate ligand and the leaving monodentate ligand L. The use of dmp instead of phen multiplied the photosubstitution efficiency by a factor of 20–50, depending on L. This effect could be qualitatively correlated to the distortions observed in the X-ray structures of the corresponding complexes. The highly distorted structure of Ru(terpy*)(dmp)(dms)$(PF_6)_2$ showed a very high photosubsitution quantum yield $\phi = 0.36$ in neat pyridine. The high photoreactivity of some of the compounds makes them particularly promising as components of future light-driven molecular machines.

Introduction

Multicomponent molecular systems which can be set in motion in a controlled fashion under the action of an external signal (molecular "machines" and "motors") are important as models of biological motors. They are also promising in relation to long-term applications in the fields of information storage and processing or nanomechanical devices.[1−5] Recently, our group has proposed a new principle to induce light-driven motion, by taking advantage of the strong dissociative character of ligand-field states (LF or d−d states) in ruthenium(II) complexes.[6−10] Provided the ligand field imposed by the set of ligands is not too strong, which can be controlled by steric factors in particular (distorted octahedral geometry), the LF state is accessible enough to be efficiently populated from the ^{3}MLCT (metal-to-ligand charge transfer) state. This process is followed by the expulsion of a given ligand and its substitution by solvent molecules or other entering ligands. Interestingly, examples of these photosubstitution reactions have been reported long ago, but they were generally considered as detrimental (degradation of photocatalysts or electron transfer relays).[11−16]

* To whom correspondence should be addressed. E-mail: jpcollin@chimie.u-strasbg.fr.

† Department of Chemistry, Trinity College, Dublin, Ireland.

(1) From a special issue on molecular machines: Collin, J.-P.; Dietrich-Buchecker, C.; Gaviña, P.; Jimenez-Molero, M. C.; Sauvage, J.-P. *Acc. Chem. Res*. **2001**, *34*, 477.
(2) Balzani, V.; Credi, A.; Raymo, F. M.; Stoddart, F. J. *Angew. Chem., Int. Ed.* **2000**, *39*, 3348.
(3) Sauvage, J.-P. *Molecular Machines and Motors, Structure & Bonding*; Springer: Berlin, 2001; Vol. 99.
(4) Feringa, B. L. *Molecular Switches*; Wiley-VCH: Weinheim, 2001.
(5) Balzani, V.; Credi, A.; Venturi, M. *Pure Appl. Chem*. **2003**, *75*, 541.
(6) Laemmel, A.-C.; Collin, J.-P.; Sauvage, J.-P. *Eur. J. Inorg. Chem*. **1999**, 383.
(7) Laemmel, A.-C.; Collin, J.-P.; Sauvage, J.-P. *C. R. Acad. Sci. Paris, Ser. IIc* **2000**, *3*, 43.
(8) Collin, J.-P.; Laemmel, A.-C.; Sauvage, J.-P. *New J. Chem*. **2001**, *25*, 22.
(9) Pomeranc, D.; Jouvenot, D.; Chambron, J.-C.; Collin, J.-P.; Heitz, V.; Sauvage, J.-P. *Chem. Eur. J*. **2003**, *9*, 4247.
(10) Arico, F.; Mobian, P.; Kern, J.-M.; Sauvage, J.-P. *Org. Lett.* **2003**, *5*, 1887.
(11) Hoggard, P. E.; Porter, G. B. *J. Am. Chem. Soc*. **1978**, *100*, 1457.
(12) Durham, B.; Caspar, J. V.; Nagle, J. K.; Meyer, T. J. *J. Am. Chem. Soc*. **1982**, *104*, 4803.
(13) Henderson, L. J.; Ollino, M., Jr.; Gupta, V. K.; Newkome, G. R.; Cherry, W. R. *J. Photochem*. **1985**, *31*, 199.

10.1021/ic0491736 CCC: $27.50
Published on Web 11/20/2004

The need for new building blocks to be incorporated in dynamic molecular systems of the catenane or rotaxane family prompted us to explore the potential of ruthenium(II) complexes of the Ru(terpy)(diimine)(L)$^{2+}$ type (terpy = 2,2′,6′,2″-terpyridine; diimine = 1,10-phenanthroline or derivative; L = neutral monodentate ligand). In the present Article, the synthesis, crystallographic study, and photochemical reactivity of a series of such complexes are reported. In particular, it has been possible to demonstrate that the use of sterically hindering bidentate chelates increases dramatically the photochemical lability of the leaving monodentate ligand as compared to complexes containing nonhindering chelates.

Results and Discussion

Due to their photochemical reactivity, complexes containing thioethers (R−S−R) or aromatic nitriles as monodentate ligand have been synthesized and investigated. For solubility reasons, 4′-(3,5-ditertiobutyl)phenyl-2,2′,6′,2″-terpyridine, abbreviated as terpy*, has been preferred to plain terpy. The bidentate chelates used are 1,10-phenanthroline (phen) and its sterically hindered analogue, 2,9-dimethyl-1,10-phenanthroline (dmp). The choice of these organic ligands has been dictated by their ease of access and by the fact that our group is familiar with the functionalization of such building blocks, which should allow us to incorporate them into more sophisticated structures in the future. The chemical formulas of the ligands and the ruthenium complexes synthesized or involved in this work are presented in Figure 1.

Synthesis of the Complexes. The complexes **1**−**10** were prepared following classical routes.[17−19] The terdentate chelate terpy* was first complexed to Ru(III) to afford Ru(terpy*)Cl_3. The bidentate chelate phen or dmp was subsequently introduced while ruthenium(III) was reduced to ruthenium(II), and the sixth ligand (Cl) was replaced by a neutral species. The sequence of reactions is indicated for each complex in Scheme 1.

All the complexes in Scheme 1 except Ru(terpy*)(dmp)(Cl)$^+$ were isolated as PF_6^- salts and characterized by ^{1}H NMR (COSY and ROESY) spectroscopy, electrospray mass spectrometry (ES-MS), and electronic absorption spectroscopy (UV−vis). These data are in agreement with their postulated structure. In addition, X-ray crystallographic studies were performed on complexes **3**, **5**, **8**, and **9**.

Crystallographic Study. Monocrystals suitable for X-ray analysis were obtained for the four complexes **3**, **5**, **8**, and **9** but not for complex **4**. Although **3** bears two methyl groups on the benzonitrile ligand and **4** bears two methoxy groups, we considered that the structure of **3** was a good model of

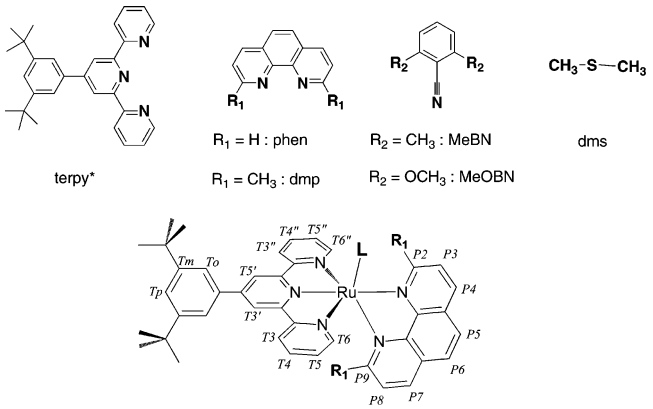

	Ru(terpy*)(phen)(Cl)$^+$:	**1**
	Ru(terpy*)(phen)(CH_3CN)$^{2+}$:	**2**
R_1 = H	Ru(terpy*)(phen)(MeBN)$^{2+}$:	**3**
	Ru(terpy*)(phen)(MeOBN)$^{2+}$:	**4**
	Ru(terpy*)(phen)(dms)$^{2+}$:	**5**
	Ru(terpy*)(phen)(py)$^{2+}$:	**6**
	Ru(terpy*)(dmp)(CH_3CN)$^{2+}$:	**7**
R_1 = CH_3	Ru(terpy*)(dmp)(MeOBN)$^{2+}$:	**8**
	Ru(terpy*)(dmp)(dms)$^{2+}$:	**9**
	Ru(terpy*)(dmp)(py)$^{2+}$:	**10**

Figure 1. Chemical formulas of the compounds synthesized.

Scheme 1

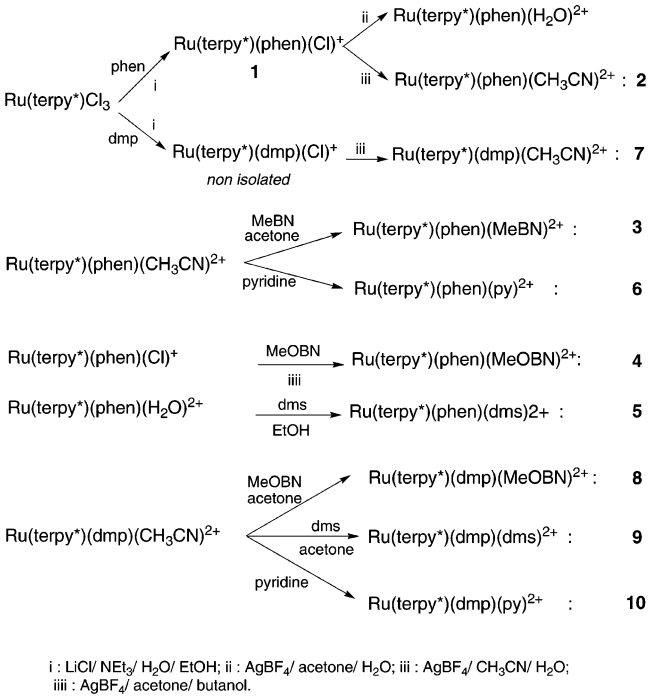

i : LiCl/ NEt_3/ H_2O/ EtOH; ii : $AgBF_4$/ acetone/ H_2O; iii : $AgBF_4$/ CH_3CN/ H_2O; iiii : $AgBF_4$/ acetone/ butanol.

4 (see below). The literature includes many X-ray structures of phenothiazine[19,20] or thio-crownethers[21] complexed on ruthenium(II) centers bearing py, bpy, or phen ligands, but **5** and **9** are among the few X-ray structures of polypyridyl ruthenium complexes bearing acyclic thioether ligands.[22] Complex **5** crystallized with two molecules in the asymmetric

(14) von Zelewsky, A.; Gremaud, G. *Helv. Chim. Acta* **1988**, *71*, 1108.
(15) Crutchley, R. J.; Lever, A. B. P. *Inorg. Chem.* **1982**, *21*, 2276.
(16) Allen, G. H.; White, R. P.; Rillema, D. P.; Meyer, T. J. *J. Am. Chem. Soc.* **1984**, *106*, 2613.
(17) Takeuchi, K. J.; Thompson, M. S.; Pipes, D. W.; Meyer, T. J. *Inorg. Chem.* **1984**, *23*, 1845.
(18) Adcock, P. A.; Keene, F. R.; Smythe, R. S.; Snow, M. R. *Inorg. Chem.* **1984**, *23*, 2336.
(19) (a) Bonnet, S.; Collin, J.-P.; Gruber, N.; Sauvage, J.-P.; Schofield, E. R. *Dalton Trans.* **2003**, 4654. (b) Fletcher, N. C.; Keene, F. R. *Dalton Trans.* **1998**, 2293.
(20) Kroener, R.; Heeg, M. J.; Deutsch, E. *Inorg. Chem.* **1988**, *27*, 558.

Table 1. Bond Lengths (Å) from the Ruthenium Ion to the Coordinating Atoms for Complexes **3**, **5**, **8**, and **9**

	3	**8**	**5**	**9**
Ru−N1	2.044(5)	2.103(7)	2.073(6) 2.072(6)	2.090(9)
Ru−N2	2.086(5)	2.133(6)	2.110(6) 2.100(6)	2.13(1)
Ru−N3	2.084(5)	2.061(6)	2.060(6) 2.077(6)	2.036(9)
Ru−N4	1.970(5)	1.970(5)	1.961(6) 1.966(6)	1.935(8)
Ru−N5	2.074(5)	2.075(7)	2.082(6) 2.074(6)	2.070(9)
Ru−N6	2.044(6)	2.024(7)		
Ru−S			2.365(2) 2.350(2)	2.397(3)

unit, each having slightly different geometries. Table 1 shows characteristic Ru−S and Ru−N distances in the four structures.

The Ru−S distances of 2.350(2), 2.365(2), and 2.397(3) Å are relatively longer than that in $Ru(NH_3)_5(CH_3SC_2H_5)^{2+}$ (2.316 Å),[23] $Ru([9]aneS_3)(py)_3^{2+}$ (2.313, 2.305, 2.306 Å),[21] and $Ru(phen)(pdto)^{2+}$ (2.312, 2.319 Å)[22] but comparable to that in $Ru(terpy)(phen)(ptz)^{2+}$ (2.375 Å),[19] *cis* and *trans* $Ru(bpy)_2(ptz)_2^{2+}$ (2.367, 2.395 and 2.350, 2.343 Å, respectively),[20] and $Ru(phen)_2((PhSCH_2)_2)^{2+}$ (2.357 Å)[24] ([9]$aneS_3$ = 1,4,7-trithiacyclononane, ptz = phenothiazine, bpy = 2,2′-bipyridine, pdto = 1,8-bis(2-pyridyl)-3,6-dithiaoctane). The slightly longer distance in **9** compared to **5** can be attributed to the steric hindrance between the methyl groups of the dmp and the methyl groups of dms. A reverse trend is observed between **3** and **8**, the Ru−N distance in the latter being 0.02 Å shorter than in the former. Although the steric hindrance of the methyl groups *ortho* to the nitrogens of the dmp ligand can easily be evidenced in complex **8** (see below), its structure shows an intramolecular hydrogen bond between one oxygen atom of the dimethoxybenzonitrile moiety (O2, see Figure 2 for atom numbering) and one hydrogen atom of the methyl group on the dmp (H12 borne by C12, the distance O2−H12 is 2.523 Å). The bending of the monodentate ligand L maximizes this H bond and shortens the Ru−L distance. In **3**, this hydrogen bond is of course not present; the dimethylbenzonitrile ligand is hence not bent, and the Ru−N distance is slightly longer (2.044 Å). In both cases, the values are comparable to the Ru−N distance in *cis*-$Ru(bpy)_2(PhCN)_2^{2+}$ (2.032 Å).[25] The crystal structures of the complexes **3**, **5**, **8**, and **9** are shown in Figure 2.

In Table 2 are reported seven torsion angles that quantitatively characterize the distortions observed in these structures. For each entry, the experimental values are given along with the value corresponding to an idealized structure where the coordination sphere of the metal is perfectly octahedral and the conjugated ligands are perfectly planar.

Entries I and II relate to the bending of the plane of the phenanthroline in the two directions perpendicular to the plane of the terpyridine. Entries III, IV, and V measure the distortion of the terpyridine from an idealized planar geometry. Entries VI and VII show the bending of the Ru−L bond induced by the steric hindrance of the phen moiety. Figure 3 gives comparative face views of the four structures looking along the Ru−N4 bond, with the ligand L in red, the phenanthroline moiety in blue, and the terpy* in gray. As can be seen in Figure 3, the distortion of the ruthenium coordination sphere increases in the order **3** < **5** < **8** < **9**. Two factors seem to play a major influence: (i) the methyl group borne by the P2 carbon atom collides with the monodentate ligand L, which induces a major steric congestion in **8** and **9** compared to **3** and **5**, respectively. For example, entry I shows a bending of the phen moiety of 0.75° for **3**, 2.70° and 7.07° for **5**, 13.61° and 23.30° for **8** and **9**, respectively. (ii) The methyl groups of the dimethyl sulfide are directly attached to the sulfur atom and hence very close to the ruthenium atom. The resulting steric congestion is greater than with L = benzonitrile because in the latter case the methyl groups in *ortho* position to the nitrile are two atoms further away. Also, the phen bending angle difference (entry II) between the ideal structures (180°) and the real complexes changes from 0.09° to 10.54° with L = benzonitrile and from 4.28/5.52° to 21.86° with L = dimethyl sulfide.

As noted elsewhere,[19,26] the distortion of the terpyridine out of its average plane (entries III−V) depends on the steric congestion described above but also on the packing and on interactions with solvent molecules within the asymmetric unit. For example, entry V shows that the congested structure of **8** has a comparatively planar terpyridine (bending angle of 1.21°) whereas its less sterically hindered analogue **3** is more distorted (4.73°). A look at the packing shows that this distortion is probably due to an H−π interaction between the hydrogen atom in *para* position to the nitrile group of the benzonitrile of one molecule and an outer pyridine of the terpyridine moiety of a neighboring molecule (see Supporting Information). The intermolecular distances between H41 and the two atoms N5 and C25 of the outer pyridine ring in **3** are 3.093 and 3.066 Å, respectively, compared to 3.190 and 3.075 Å in **8** (the atoms are H17, N3, and C34 in this structure). Moreover, the angle between the C20−H17 bond and the average plane of the pyridine in **8** is shorter (55°) than in **3** between the C46−H41 bond and the corresponding pyridine plane (72°). The H−π interaction is hence higher in **3** than in **8**, inducing a stronger distortion of the terpy in the former. As it seems reasonable to assume that the distortion in **4** is roughly equivalent to that in **3**, we can anticipate some correlations between the distortions in

(21) (a) Roche, S.; Adams, H.; Spey, S. E.; Thomas, J. A. *Inorg. Chem.* **2000**, *39*, 2385. (b) Madureira, J.; Santos, T. M.; Goodfellow, B. J.; Lucena, M.; de Jesus, J. P.; Santana-Marques, M. G.; Drew, M. G. B.; Félix, V. *Dalton Trans.* **2000**, 4422. (c) Goodfellow, B. J.; Pacheco, S. M. D.; de Jesus, J. P.; Félix, V.; Drew, M. G. B. *Polyhedron* **1997**, *16*, 3293.

(22) Ortiz-Frade, L. A.; Ruiz-Ramirez, L.; Gonzalez, I.; Marin-Becerra, A.; Alcarazo, M.; Alvarado-Rodriguez, J. G.; Moreno-Esparza, R. *Inorg. Chem.* **2003**, *42*, 1825.

(23) Krogh-Jespersen, K.; Zhang, X.; Ding, Y.; Westbrook, J. D.; Potenza, J. A.; Schugar, H. J. *J. Am. Chem. Soc.* **1992**, *114*, 4345.

(24) Jouvenot, D. Ph.D. Thesis, Université Louis Pasteur, Strasbourg, France, June 2004.

(25) Griffith, W. P.; Reddy, B.; Shoair, A. G. F.; Suriaatmaja, M.; White, A. J. P.; Williams, D. J. *Dalton Trans.* **1998**, 2819.

(26) Rasmussen, S. C.; Ronco, S. E.; Mlsna, D. A.; Billadeau, M. A.; Pennington, W. T.; Lolis, J. K.; Petersen, J. D. *Inorg. Chem.* **1995**, *34*, 821.

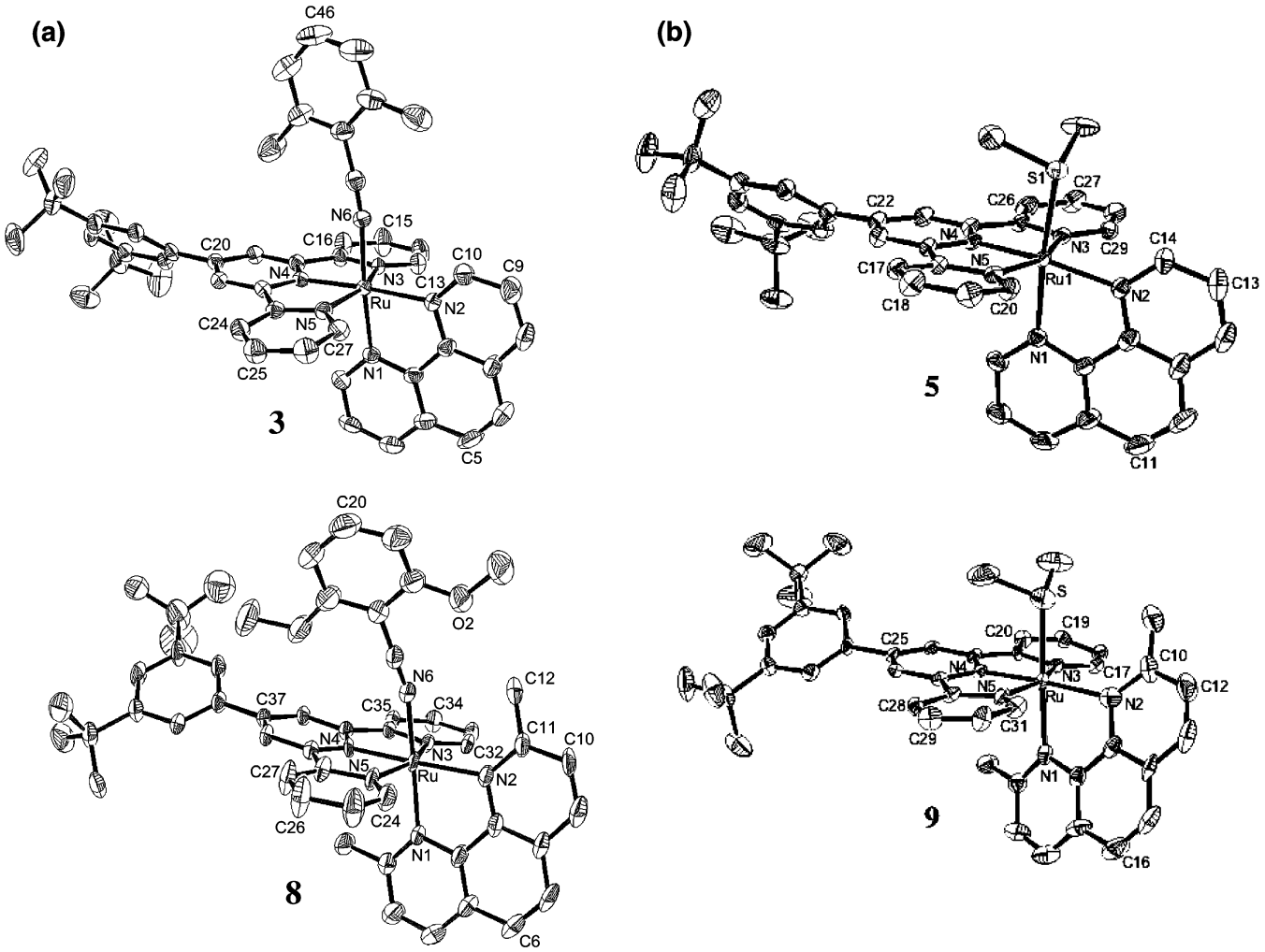

Figure 2. (a) Face views of the crystal structures of complexes **3** and **4**. Solvent molecules, H atoms, and anions are omitted for clarity. Ellipsoids are scaled to enclose 50% of the electronic density. (b) The same for complexes **5** and **9**.

Table 2. Characteristic Bending Angles in Complexes **3**, **5**, **8**, and **9**

		experimental values			
	idealized values[a]	**3**	**5**[b]	**8**	**9**
I	0°	RU−N1−C5−C9 0.75	RU1−N1−C11−C13/RU2−N6−C53−C47 2.70/7.07	RU−N1−C6−C10 13.61	RU−N1−C16−C12 23.30
II	180°	RU−N1−N2−C5 179.91	RU1−N1−N2−C11/RU2−N6−N7−C53 175.72/174.48	RU−N1−N2−C6 169.46	RU−N1−N2−C16 158.14
III	0°	C20−N4−N5−C25 12.37	C22−N4−N5−C18/C65−N9−N10−C70 7.93/0.78	C37−N4−N5−C26 6.76	C25−N4−N5−C29 4.95
IV	0°	C20−N4−N3−C15 6.97	C22−N4−N3−C27/C65−N9−N8−C60 5.38/3.16	C37−N4−N3−C34 10.61	C25−N4−N3−C19 2.38
V	0°	C27−C24−C16−C13 4.73	C20−C17−C26−C29/C72−C69−C61−C58 1.85/7.64	C24−C27−C35−C32 1.21	C31−C28−C20−C17 11.22
VI	180°	N6−RU−N2−N1 179.60	S1−RU1−N2−N1/S2−RU2−N7−N6 177.24/178.57	N6−RU−N2−N1 172.20	S−RU−N2−N1 173.68
VII	0°	N6−RU−N2−C10 1.34	S1−RU1−N2−C14/S2−RU2−N7−C46 4.92/5.95	N6−RU−N2−C11 16.46	S−RU−N2−C10 16.33

[a] See text. [b] Two distinct molecules in the unit cell.

the crystal structures of **3** and **8** and the photochemical reactivity of complexes **4** and **8**.

Spectroscopic Properties. Table 3 gives the ^{1}MLCT absorption bands of complexes **4**, **5**, **6**, **8**, **9**, and **10** in pyridine, and as previously observed, the identity of the ligand at the sixth coordination site in the complexes can strongly influence the position of this absorption band.[19] As can be seen, the wavelength maxima increase in both series (phen and dmp) in the order MeOBN < dms < py. The increasing σ-donor properties of these ancillary monodentate ligands increase the energy of the t_{2g} orbital centered on the ruthenium atom and hence decreases the energy needed to promote an electron from these orbitals to the π^* orbital centered on the polypyridyl ligands. In addition, the π acceptor character of the ligands diminishes in the series, which is also in agreement with the experimental observa-

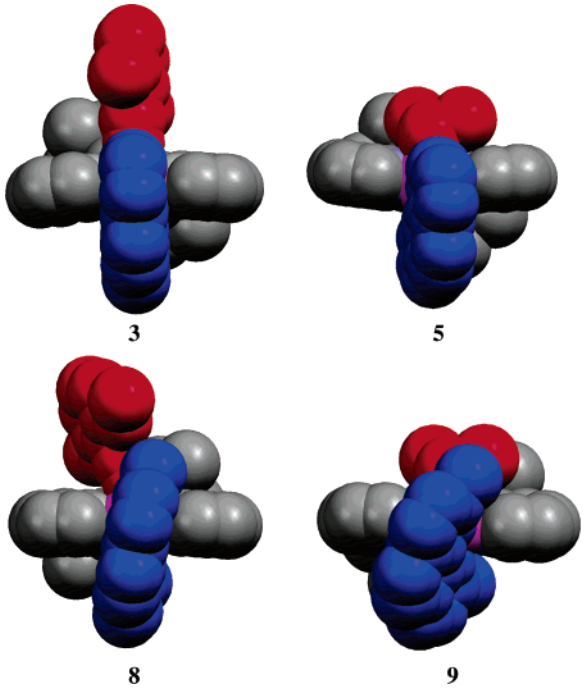

Figure 3. View of the crystal structure of complexes **3**, **5**, **8**, and **9** in space-filling representation.

Table 3. Absorption Data for ^{1}MLCT Bands of Selected Complexes in Pyridine

complexes	λ_{MLCT} (nm)/ϵ_{MLCT} ($\times 10^3$ L·mol^{-1}·cm^{-1})
4	465/15.2
5	473/11.5
6	487/13.2
8	467/12.4
9	492/9.84
10	495/11.9

tions. For a particular ligand L, the evolution of the absorption maxima always follows the order phen < dmp. The two methyl groups of the dmp indeed increase the σ-donor properties of the latter chelate, which reduces the energy difference between t_{2g} and π^* orbitals of the terpyridine unit.

Photoreactivity

The photochemical reactivity of the complexes **4**, **5**, **8**, and **9** has been investigated on the basis of previous work concerning the photosubstitution reactions taking place in Ru(terpy)(bidentate)(L)$^{n+}$ type complexes.[7,27,28] It has been shown that the monodentate ligand L can be selectively and quantitatively expelled by light irradiation into the MLCT absorption band and replaced by CH_3CN or pyridine used as solvent S (eq 1).

$$\mathrm{Ru(terpy)(N{-}N)(L)^{2+} + S \xrightarrow{h\nu} Ru(terpy)(N{-}N)(S)^{2+} + L} \quad (1)$$

The scope of this photochemical reaction has recently been demonstrated by the photochemical synthesis of various polypyridine ruthenium(II) complexes.[19] In order to test the classical assumption that the photosubsitution mechanism is dissociative, it was necessary to find a poorly coordinating solvent in which the effect of the concentration of the entering ligand on the reaction rate could be measured. The best candidate was nitromethane: the visible spectrum of a solution of **8** in degassed $MeNO_2$ did not show any modification after 10 min of irradiation. Deaerated nitromethane solutions of Ru(terpy*)(dmp)$(CH_3CN)^{2+}$ were irradiated in the presence of 3,5-lutidine in excess to maintain pseudo-first-order conditions. As shown by spectrophotometric monitoring, clear isosbestic points were observed in each case, and the calculated rate constants were found independent of the concentration. The photosubstitution first-order rate constants were also determined using different solvents as entering ligands (benzonitrile, pyridine, dmso, dms). Although their binding affinities for ruthenium(II) were different, we found relatively close values for the rate constants of the photosubsitution reaction of MeOBN by a solvent molecule. These results are in good agreement with previous studies demonstrating that photosubstitution proceeds by a dissociative mechanism in ruthenium(II) polypyridine complexes.[7,27,29]

Quantum Yield Measurements. In order to better characterize the photoreactivity of complexes of the type Ru(terpy*)(N−N)(L)$^{2+}$, the quantum yields of the photosubstitution reactions of L by pyridine were measured for the complexes **4**, **8**, and **9** in neat pyridine (Scheme 2).

McMillin et al. published the quantum yield for the same reaction performed on the complex Ru(terpy)(bpy)$(CH_3CN)^{2+}$ but using a 1 M solution of pyridine in acetonitrile as the solvent.[27] To compare our own results to this previous work, we also measured the quantum yield of the photosubstitution reaction of acetonitrile by pyridine in the analogous complex Ru(terpy)(phen)$(CH_3CN)^{2+}$.[19] Table 4 gives the quantum yields for the five complexes.

As expected, the photosubstiution quantum yield for complex Ru(terpy)(phen)$(CH_3CN)^{2+}$ was found to be very close ($\phi = 0.0016$) to the value previously reported in the case of its bipyridine analogue ($\phi = 0.0013$). Changing simultaneously acetonitrile for benzonitrile (MeOBN), terpy for terpy*, and the solvent did not change significantly the order of magnitude of the photosubsitution quantum yield ($\phi = 0.0035$). However, a dramatic change was observed when, leaving all other conditions unchanged, the bidentate phen was replaced by its hindered derivative dmp. Although steric hindrance was introduced on a spectator ligand and not on the leaving monodentate ligand, once the complex was formed it was redistributed in an overall fashion within the coordination sphere of the ruthenium atom. As a result, the photoejection quantum yield became 22 times higher for **8** ($\phi = 0.079$) than for **4** and reached the same order of magnitude as the photoejection quantum yield of the hindered chelate 6,6′-dimethyl-2,2′-bipyridine (dmbp) in the complex

(27) Hecker, C. R.; Fanwick, P. E.; McMillin, D. R. *Inorg. Chem.* **1991**, *30*, 659.
(28) Schofield, E. R.; Collin, J.-P.; Gruber, N.; Sauvage, J.-P. *Chem. Commun.* **2003**, 188.
(29) Durham, B.; Caspar, J. V.; Nagle, J. K.; Meyer, T. J. *J. Am. Chem. Soc.* **1982**, *104*, 4803.

Scheme 2

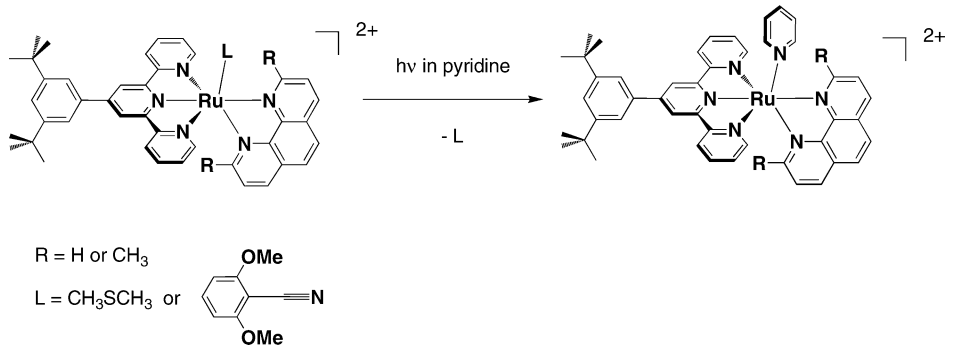

Table 4. Quantum Yield for the Photosubstitution Reactions of L by Pyridine[a]

complexes	L	solvent	excitation wavelength	quantum yield
$Ru(tpy)(bpy)(CH_3CN)^{2+}$ [b]	CH_3CN	pyridine 1 M in acetonitrile	464	0.0013 ± 0.0001
$Ru(tpy)(phen)(CH_3CN)^{2+}$ [c]	CH_3CN	pyridine 1 M in acetonitrile	464	$0.0016 \pm 0.0\ 002$
$Ru(tpy^*)(phen)(MeOBN)^{2+}$ ($\mathbf{4}^{2+}$)	MeOBN	neat pyridine	476	0.0035 ± 0.0009
$Ru(tpy^*)(dmp)(MeOBN)^{2+}$ ($\mathbf{8}^{2+}$)	MeOBN	neat pyridine	476	0.079 ± 0.015
$Ru(tpy^*)(dmp)(dms)^{2+}$ ($\mathbf{9}^{2+}$)	dms	neat pyridine	513	0.36 ± 0.11

[a] All measurements were done at 25 °C on PF_6^- salts. [b] See ref 27. [c] Prepared according to ref 19.

$Ru(phen)_2(dmbp)^{2+}$ ($\phi = 0.020$).[30] Keeping dmp as the bidentate ligand but changing L to dimethyl sulfide, the quantum yield was multiplied still further by a factor of 4.5 to reach the value $\phi = 0.36$ for complex **9**. This value is rather unusual for a ruthenium(II) polypyridyl complex.

We can qualitatively correlate the evolution of the photosubsitution quantum yields in the series **4** < **8** < **9** to the evolution of the torsion angles between the plane of the phenanthroline and the ideal plane perpendicular to the terpyridine. Entries I and II of Table 2 give increasing values of 0.75 °< 13.61° < 23.30° and decreasing values of 179.91° > 169.46° > 158.14°, respectively. By replacing phen by dmp and MeOBN by dms, the steric demand around the ruthenium center increases because of the increasing interaction with the methyl group borne by the P2 carbon atom of the phenanthroline moiety (see above). Doing so, the ligand field of the complex is decreased, which reduces the energy gap between the antibonding metal-centered e_g and ligand-centered π^* orbitals. It cannot be excluded that the ^{3}MLCT state will be also affected by distortion. Overall, the photogenerated ^{3}MLCT state will approach the dissociative ^{3}d−d metal-centered excited state, leading to a higher photoexpulsion efficiency.

Kinetic Experiments. Quantitative data concerning photoreactivity requires determination of quantum yields using a monochromator. By contrast, white light irradiation experiments only lead to indicative data, as far as kinetic properties are concerned; however, they are simple to perform and very useful for preparative purposes.[19] Experiments using the latter technique showed that when the concentration of the complex was kept low ($C = 10^{-5}$ mol·L^{-1}) and the incoming ligand was the solvent, the final state was characterized by a complete conversion. The absorption spectra recorded versus time displayed well-defined isosbestic points (Figure 4 a).

The plots of $\ln[(A_0 - A_\infty)/(A_t - A_\infty)]$ versus time were linear, and the pseudo-first-order rate constants reported in Table 5 were calculated using least-squares treatment. Kinetic data at room temperature are given in Table 5 for complexes **4**, **5**, **8**, and **9**.

The reaction was also monitored by ^{1}H NMR spectroscopy using d_5-pyridine as the solvent. The ^{1}H NMR spectrum of **8** displays in the 6.10−6.90 ppm region a doublet assigned to the aromatic protons of MeOBN in the *meta* position. After complete irradiation, this signal vanished and was replaced by the characteristic signal of the protons of an uncoordinated MeOBN in C_5D_5N indicating that the photosubstitution was selective and quantitative (Figure 4b).

These simple experiments qualitatively confirmed the quantum yield values. In compounds **8** and **9**, the presence of methyl groups in P2 and P9 positions of the phenanthroline ligand increased the photosubstitution rates as compared to those of compounds **4** and **5** by a factor 9 and 60, respectively. The more distorted situation, as evidenced by the X-ray crystal structure of **9**, leads to the fastest reaction ($k = 0.140$ s^{-1}). The reaction was also performed for complex **5** and showed a moderate photochemical efficiency, between the values found for complexes **4** and **8**. The qualitative correlation between quantum yield values and distortion angles in the X-ray structures (see above) can be generalized to the whole series of complexes **4**, **5**, **8**, and **9** using the first-order rate constants *k* obtained in white light irradiation experiments.

Such an increase of the reactivity was previously reported for the thermal substitution of the aqua ligand by acetonitrile in a series of Ru(terpy)(bidentate ligand)$(H_2O)^{2+}$ complexes and allowed to give a quantitative estimation of steric ligand effects for bidentate bipyridyl ligands.[31] In other work, the

(30) Laemmel, A.-C.; Collin, J.-P.; Sauvage, J.-P.; Accorsi, G.; Armaroli, N. *Eur. J. Inorg. Chem.* **2003**, 467.

(31) Bessel, C. A.; Margarucci, J. A.; Acquaye, J. H.; Rubino, R. S.; Crandall, J.; Jircitano, A. J.; Takeuchi, K. J. *Inorg. Chem.* **1993**, *32*, 5779.

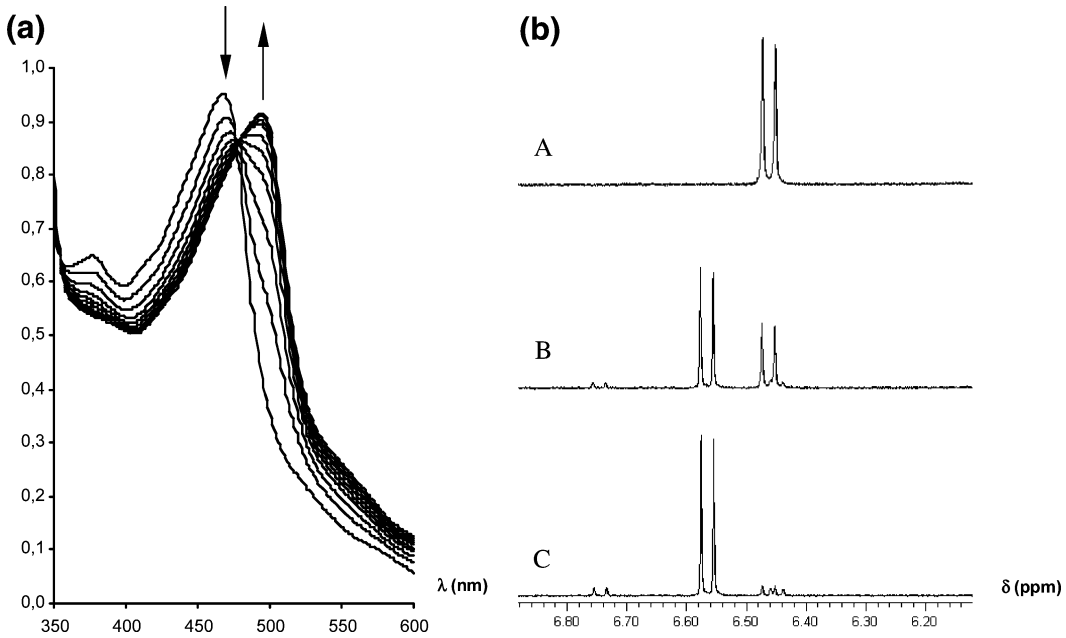

Figure 4. (a) Time evolution of visible spectrum of **8** irradiated in pyridine. One curve every 20 s. (b) Time evolution of the proton 300 MHz NMR spectrum of **8** irradiated in C_5D_5N: A, $t = 0$; B, $t = 5$; C, $t = 20$ min. Region: $\delta = 6.90-6.10$ ppm (aromatic proton in meta position of the nitrile group in MeOBN).

Table 5. Kinetic Data of White Light Irradiation Experiments in Neat Pyridine

complex	relative rate constant k^a	$t_{1/2}$ (s)
4	1	307
5	1.46	211
8	8.67	35.4
9	61.9	4.95

[a] Value for complex **4**: $k_{subst} = 0.00226\ s^{-1}$.

same group described a similar effect on *fac*-Ru(tpmm)-(bidentate)$(H_2O)^{2+}$ complexes (tpmm = tris(2-pyridyl)-methoxymethane).[32] For some tris chelate complexes of ruthenium(II), it was demonstrated that the photosubstitution quantum yields were closely related to the energy gap law.[33] In other cases, the photoreactivity depends also on steric factors.[14] In the present study, it has been possible to correlate the photoreactivity of the complexes in solution with some characteristic dihedral angles found in the solid-state structures. The possibility of controlling the rate of photosubstitution reactions by steric adjustment could be of particular interest in the design of molecular machines based on photochemical processes.

Experimental Section

Single crystal X-ray diffraction experiments were carried out using Kappa CCD and graphite-monochromated Mo Kα radiation ($\lambda = 0.71073$ Å). For all computations, the MolEN package was used,[34a] and structures were drawn using ORTEP[34b] and Mercury.[34c] Crystal data and details of data collection for complexes **3**, **5**, **8**, and **9** are provided in Table 6. In the case of **5** and **8**, the positions of the solvent molecules are poorly defined because the solvents used for crystallization were very volatile. However, the structure of the complex itself is determined with good accuracy.

^{1}H NMR spectra were acquired on either a Bruker WP200 SY (200 MHz), a Bruker AVANCE 300 (300 MHz), or a Bruker AVANCE 400 (400 MHz) spectrometer, using the deuterated solvent as the lock and residual solvent as the internal reference. Mass spectra were obtained by using a VG ZAB-HF(FAB) spectrometer or a VG-BIOQ triple quadrupole, positive mode (ES-MS). UV−vis spectra were recorded with a Kontron Instruments UVIKON 860 spectrometer at room temperature.

Quantum Yield Measurements. Quantum yields were determined using the excitation system of an Aminco Bowman series 2 luminescence spectrophotometer (Thermospectronic). This irradiation system consisted of a continuous wave 150 W xenon lamp with a monochromator using a 1200 lines/mm, ion etched, concave, holographic gratings in a modified Seya−Namioka design with 200 mm focal length. The aperture of the monochromator was computer-set to $\Delta\lambda = 8$ nm. The sample was immobilized in a T-Optics standardized sample chamber equipped with an SLM Aminco magnetic stirrer and thermostated to 25 °C by a Bioblock Scientific Polystat 5 number 86613. The sample was made of 3 mL of the solution of the compound put in a closed, UV−vis glass cell with a 1.00 cm path length under an air atmosphere. To avoid the influence of external light, the room was kept in the dark for the duration of the experiments. Under these conditions, the light intensities were determined using ferrioxalate actinometry.[35] See Supporting Information for more detailed data.

White Light Irradiation Experiments. A pyridine solution (3 mL) of the complex ($C = 10^{-5}$ M) was put in a closed UV−vis glass cell. The sample was irradiated with the beam of a 250 W

(32) Huynh, M. H. V.; Lasker, J. M.; Wetzler, M.; Mort, B.; Szczepura, L. F.; Witham, L. M.; Cintron, J. M.; Marschilok, A. C.; Ackerman, L. J.; Castellano, R. K.; Jameson, D. L.; Churchill, M. R.; Jircitano, A. J.; Takeuchi, K. J. *Angew. Chem., Int. Ed.* **2001**, *40*, 4469.
(33) Ross, H. B.; Boldaji, M.; Rillema, P. D.; Blanton, C. B.; White, R. P. *Inorg. Chem.* **1989**, *28*, 1013.
(34) (a) Fair, C. K. In *MolEN, An interactive intelligent system for crystal structure analysis*; Nonius: Delft, The Netherlands, 1990. (b) Johnson, C. K. *ORTEP-II: A FORTRAN Thermal Ellipsoid Plot Program for Crystal Structure Illustrations*; Report ORNL-5138; Oak Ridge National Laboratory: Oak Ridge, TN, 1976. (c) http://www.ccdc.cam.ac.uk/products/csd_system/mercury/.
(35) Calvert, J. G.; Pitts, J. N. *Photochemistry*; Wiley & Sons: New York, 1967; p 783.

Table 6. Crystallographic Data for **3**, **5**, **8**, and **9**

	3	**5**	**8**	**9**
formula	$C_{50}H_{48}N_6Ru\cdot 2PF_6\cdot C_2H_6O$	$C_{172}H_{180}N_{20}Ru_4S_4\cdot 8PF_6\cdot 3H_2O\cdot 6C_2H_4Cl_2$	$C_{104}H_{104}N_{12}O_4Ru_2\cdot 4PF_6\cdot 4C_3H_6O\cdot C_4H_{10}O$	$C_{45}H_{49}N_5RuS\cdot 2PF_6\cdot CH_2Cl_2$
mol wt	1170.05	4867.55	2674.51	1167.92
cryst syst	monoclinic	triclinic	triclinic	monoclinic
space group	*C*2/*c*	$P\bar{1}$	$P\bar{1}$	$P2_1/c$
a (Å)	25.0624(2)	11.0983(1)	14.3343(5)	12.7000(3)
b (Å)	13.6912(2)	20.9631(3)	15.8785(5)	23.4037(5)
c (Å)	33.6533(4)	23.8225(3)	15.9528(6)	17.3218(4)
α (deg)	90	84.056(5)	108.482(5)	90
β (deg)	107.386(5)	79.303(5)	102.042(5)	103.614(5)
γ (deg)	90	87.692(5)	96.712(5)	90
V (Å^3)	11020.0(2)	5415.6(1)	3301.7(2)	5003.9(2)
Z	8	1	1	4
color	orange	red	orange	red
D_{calcd} (g cm^{-3})	1.41	1.49	1.35	1.55
μ (mm^{-1})	0.425	0.615	0.368	0.610
T/K	173	173	173	173
R^a	0.062	0.077	0.082	0.087
$R_w{}^b$	0.087	0.097	0.096	0.102

[a] $R = \sum||F_o| - |F_c||/|F_o|$. [b] $R_w = [\sum w(|F_o| - |F_c|)^2/\sum w(|F_o|^2)]^{1/2}$.

slide projector, filtered by a water filter, and focused on the cell. The evolution of the absorption spectrum of the solution was followed with respect to irradiation time. The plots of $\ln[(A_0 - A_\infty)/(A_t - A_\infty)]$ versus time were linear, and the pseudo-first-order rate constants were calculated using least-squares treatment.

Syntheses. Pyridine was distilled and kept over KOH. MeBN, MeOBN, phen, dmp, dms, acetonitrile were commercial products. KPF_6 was used as a 40 g/L aqueous solution. Ru(terpy*)Cl_3, Ru(terpy*)(phen)$(H_2O)(PF_6)$, **1**, and **2** were prepared following literature procedures.[19]

Ru(terpy*)(phen)(MeBN)$(PF_6)_2$. There were 22.5 mg (0.0217 mmol) of **2** and 28.5 mg (0.218 mmol) of 2,6-dimethylbenzonitrile dissolved in 5 mL of acetone. The solution was degassed and refluxed under argon overnight. The solution was cooled to room temperature, the volume of acetone was reduced to 2 mL, and 10 mL of KPF_6 was added. The solid was filtered, washed with water and ether, and put on a silica gel column (eluent: acetone/water/KNO_3 480:20:1). To the collected fractions was added KPF_6, acetone was removed and the solid filtered, washed, and dried. Yield: 16.6 mg of **3** (68%). Monocrystals were grown by slow vapor diffusion of diisopropyl ether in acetone. ^{1}H 300 MHz NMR δ (ppm) in acetone-d_6: 10.36 (dd, 1H, P_2); 9.25 (s, 2H, $T_{3'5'}$); 9.11 (dd, 1H, P_4); 8.94 (m, 2H, $T_{33''}$); 8.64 (dd, 1H, P_7); 8.53 (d, 1H, P_5); 8.51 (dd, 1H, P_3); 8.34 (d, 1H, P_6); 8.26 (dd, 1H, P_9); 8.17 (td, 2H, $T_{44''}$); 8.04 (d, 2H, T_o); 8.02 (dm, 2H, $T_{66''}$); 7.78 (t, 1H, T_p); 7.41 (dd, 1H, P_8); 7.46−7.40 (3H, $T_{55''}$ and B_p); 7.17 (d, 2H, B_m, $^3J_{m-p} = 7.7$ Hz); 2.13 (s, 6H, CH_3(B)); 1.48 (s, 18H, CH_3(^{t}Bu)). In the notation, B stands for the ligand 2,6-dimethylbenzonitrile.

Ru(terpy*)(phen)(MeOBN)$(PF_6)_2$. There were 25 mg of **1** (0.0283 mmol) and 5.7 mg of $AgBF_4$ (1 equiv, 0.0283 mmol) dissolved in 40 mL of acetone dried over $MgSO_4$. The solution was degassed and refluxed under argon for 1 h. The cooled solution was filtered, 3 equiv (17 mg) of silver tetrafluoroborate were added along with 552 mg of 2,6-dimethoxybenzonitrile (120 equiv) and 40 mL of *n*-butanol dried over $MgSO_4$. Acetone was evaporated, and the butanol solution was refluxed under argon for 4 h. The cool solution was filtered over Celite and the butanol removed under vacuum. Acetone and then 20 mL of KPF_6 and 20 mL of water were added, the acetone was evaporated, and the solid was filtered, washed with water, Et_2O, dried, and purified by column chromatography (SiO_2, eluent acetone/water/KNO_3 400:5:0.1). The last fraction was collected, 30 mL of KPF_6 were added, acetone was evaporated, and the solid was filtered, washed, and dried. Yield: 21.9 mg of **4** (67%). ^{1}H 300 MHz NMR δ (ppm) in acetone-d_6: 10.26 (dd, 1H, P_2); 9.26 (s, 2H, $T_{3'5'}$); 9.11 (dd, 1H, P_4); 8.92 (m, 2H, $T_{33''}$); 8.63 (dd, 1H, P_7); 8.56 (dd, 1H, P_3); 8.53 (dd, 1H, P_5); 8.34 (d, 1H, P_6); 8.25 (dd, 1H, P_9); 8.15 (td, 2H, $T_{44''}$); 8.09 (d, 2H, T_o); 7.94 (dm, 2H, $T_{66''}$); 7.81 (t, 1H, T_p); 7.66 (dd, 1H, P_8); 7.57 (t, 1H, B_p, $^3J_{p-m} = 8.6$ Hz); 7.41 (m, 2H, $T_{55''}$); 6.73 (d, 2H, B_m, $^3J_{m-p} = 8.6$ Hz); 3.82 (s, 6H, OMe(B)); 1.50 (s, 18H, CH_3(^{t}Bu)). In the notation, B stands for the ligand 2,6-dimethoxybenzonitrile. ES-MS *m*/*z* (calcd): 1011.3 (1011.3, $[M - PF_6]^+$), 433.0 (433.2, $[M - 2PF_6]^{2+}$). UV−vis: in pyridine $\lambda_{max} = 465$ nm (15200).

Ru(terpy*)(phen)(dms)$(PF_6)_2$. There was 16.3 mg of Ru(terpy*)(phen)$(H_2O)(PF_6)_2$ (0.0161 mmol) dissolved in a mixture of 2 mL of dimethyl sulfide and 10 mL of ethanol, and the solution was degassed and refluxed under argon for 2 h. The solvents were evaporated, and the solid residue was purified by chromatography on silica gel in the dark (eluent: acetone/water/KNO_3 60:5:0.5) to yield quantitatively an orange complex. Monocrystals suitable for X-ray analysis were obtained by slow diffusion, in the absence of light, of ^{i}Pr$_2$O in 1,2-dichloroethane. ^{1}H 300 MHz NMR δ (ppm) in acetone-d_6: 10.30 (d, 1H, P_2); 9.29 (s, 2H, $T_{3'5'}$); 9.10 (d, 1H, P_4); 9.95 (dd, 2H, $T_{33''}$); 8.65 (dd, 1H, P_7); 8.51 (d + dd, 2H, P_3 + P_5); 8.33 (d, 1H, P_6); 8.16 (td, 2H, $T_{44''}$); 8.09 (d + d, 3H, P_9 +T_o); 7.92 (d, 2H, $T_{66''}$); 7.81 (t, 1H, T_p); 7.67 (dd, 1H, P_8); 7.40 (m, 2H, $T_{55''}$); 1.66 (s, 6H, $(CH_3)_2S$); 1.49 (s, 18H, tBu). Anal. Calcd for $C_{43}H_{45}F_{12}N_5P_2Ru$: C, 48.96; H, 4.30; N, 6.64. Found: C, 48.55; H, 4.70; N, 6.31.

Ru(terpy*)(phen)(py)$(PF_6)_2$. There was 35.1 mg of **2** (0.0340 mmol) dissolved into 10 mL of neat pyridine and refluxed under argon for 2 h. The pyridine was removed under vacuum, acetone was added, and the complex was precipitated with aqueous KPF_6. The solid was filtered, washed with water, recovered with acetone, and dried under vacuum to quantitatively yield **6**. ^{1}H 300 MHz NMR δ (ppm) in acetone-d_6: 9.42 (dd, 1H, P_2); 9.19 (s, 2H, $T_{3'5'}$); 9.07 (dd, 1H, P_4); 8.91 (dm, 2H, $T_{33''}$); 8.59 (dd, 1H, P_7); 8.52 (d, H, P_5); 8.39 (dd, 1H, P_3); 8.33 (d, 1H, P_6); 8.24 (m, 2H, PY_o); 8.14 (td, 2H, $T_{44''}$); 8.12 (dd, 1H, P_9); 8.01 (d + dm, 4H, T_o + $T_{66''}$); 7.97 (tt, 1H, PY_p); 7.77 (t, 1H, T_p); 7.61 (dd, 1H, P_8); 7.43 (m, 4H, $T_{55''}$ + PY_m); 1.47 (s, 18H, tBu). ES-MS *m*/*z* (calcd): 391.15 (391.13, $[M - 2PF_6]^{2+}$). Anal. Calcd for $C_{46}H_{44}F_{12}N_6P_2Ru$: C, 51.54; H, 4.14; N, 7.84. Found: C, 51.55; H, 4.29; N, 7.61.

Ru(terpy*)(dmp)$(CH_3CN)(PF_6)_2$. There were 100 mg of Ru(terpy*)Cl_3 (0.159 mmol), 36.5 mg of hemiaqua-2.9-dimethyl-1,10-phenanthroline (1.1 equiv, 0.175 mmol), and 33.7 mg of lithium

chloride (5 equiv, 0.80 mmol) mixed with 0.5 mL of triethylamine, 10 mL of water and 30 mL of ethanol were added, and the solution was degassed and refluxed under argon for 4 h 15 min. To the cooled dark reddish solution was added 20 mL of KPF_6 and 20 mL of water. The ethanol was evaporated and the violet precipitate filtered and washed twice with water and once with ether. Careful column chromatography performed in relative darkness (SiO_2, eluent: acetone/water/KNO_3 125:5:0.1) yielded 100 mg of a mixture of the hydroxy and chloro complexes. This mixture was used without further purification. To the 100 mg (0.110 mmol) of product were added 32 mg of $AgBF_4$ (1.5 equiv, 0.165 mmol), 10 mL of water, and 40 mL of acetonitrile. The solution was degassed and refluxed under argon for 15 min. Silver chloride was removed by filtration over Celite, 20 mL KPF_6 was added, and acetonitrile was evaporated. The solid was washed with water and ether, and vacuum-dried. Yield: 93 mg of **7** (80%). ^{1}H 400 MHz NMR δ (ppm) in acetonitrile-d_3: 8.77 (s, 2H, $T_{3'5'}$); 8.75 (dd, 1H, P_4, $^3J_{3-4}$ = 8.7 Hz); 8.64 (dq, 2H, $T_{33''}$, $^3J_{33''-44''}$ = 8.1 Hz, $^5J_{33''-55''}$ = 0.7 Hz); 8.26 (d, 1H, P_7, $^3J_{7-8}$ = 8.2 Hz); 8.23 (d, 1H, P_5, $^3J_{5-6}$ = 8.7 Hz); 8.13 (d, 1H, P_6, $^3J_{6-5}$ = 8.4 Hz); 8.03 (d, 1H, P_3); 8.04 (td, 2H, $T_{44''}$, $^3J_{44''-33''}$ = $^3J_{44''-55''}$ = 7.9 Hz, $^5J_{44''-66''}$ = 1.5 Hz); 7.92 (d, 2H, T_o, $^4J_{o-p}$ = 1.8 Hz); 7.77 (t, 1H, T_p, $^4J_{p-o}$ = 1.8 Hz); 7.64 (dq, 2H, $T_{66''}$, $^3J_{66''-55''}$ = 5.6 Hz, $^5J_{66''-44''}$ = 0.7 Hz); 7.30 (2dd, 2H, $T_{55''}$, $^3J_{55''-66''}$ = 5.6 Hz, $^3J_{55''-44''}$ = 7.7 Hz, $^5J_{55''-33''}$ = 1.3 Hz); 7.29 (d, 1H, P_8, $^3J_{8-7}$ = 8.4 Hz); 3.25 (s, 3H, $CH_3(P_2)$); 1.88 (s, 3H, $CH_3(P_9)$); 1.50 (s, 18H, $CH_3(^tBu)$). The methyl group of coordinated CH_3CN is lost behind the residual solvent peak. ^{1}H 300 MHz NMR δ (ppm) in DMSO-d_6: the three methyl peaks integrate for 3H and are seen at 3.24 (P_2), 1.83 (P_9), and 2.21 (coordinated CH_3CN). ^{1}H 300 MHz NMR δ (ppm) in acetone-d_6 for comparison with other complexes (without coupling constants): 9.19 ($T_{3'5'}$); 8.90 (P_4 and $T_{33''}$, not resolved); 8.44 (P_7); 8.36 (P_5); 8.29 (P_6); 8.18 ($T_{44''}$); 8.17 (P_3); 8.08 (T_o); 7.95 ($T_{66''}$); 7.80 (T_p); 7.47 (P_8); 7.47 ($T_{55''}$); 3.44 ($CH_3(P_2)$); 2.24 (CH_3CN); 1.49 ($CH_3(^tBu)$). The $CH_3(P_9)$ is lost behind the residual solvent peaks. ^{13}C 400 MHz NMR δ (ppm) in acetonitrile d_3, assignments given by HETCORR ^{1}H−^{13}C experiments (HMQC−HMBC): 154.8 ($T_{66''}$), 139.4 ($T_{44''}$), 138.2 (P_4), 138.2 (P_7), 128.8 ($T_{55''}$), 128.2 (P_3), 128.0 (P_5), 127.8 (P_6), 127.7 (P_8), 125.8 and 125.6 (T_p and $T_{33''}$), 123.3 and 123.3 (T_o and $T_{3'5'}$), 36.0 ($C^{IV}(^tBu)$), 31.7 ($CH_3(^t$-Bu)), 28.6 ($CH_3(P_2)$), 24.8 ($CH_3(P_9)$), 4.5 (CH_3 of coordinated acetonitrile). The peaks at 160.1 and 159.7 were attributed to the P_2 and P_9 aromatic quaternary carbons. The nine remaining aromatic quaternary peaks could not be attributed: 167.8, 153.5, 151.5, 149.6, 148.7, 137.4, 130.5, 130.0, 127.3. ES-MS *m*/*z* (calcd): 917.3 (917.3, $[M - PF_6]^+$), 771.3 (772.3, $[M - 2PF_6]^+$), 731.3 (731.3, $[M - 2PF_6 - CH_3CN]^+$), 386.0 (386.1, $[M - 2PF_6]^{2+}$), 365.5 (365.6, $[M - 2PF_6 - CH_3CN]^{2+}$). Anal. Calcd for $C_{45}H_{46}F_{12}N_6P_2Ru$: C, 50.90; H, 4.37; N, 7.91. Found: C, 50.43; H, 4.52; N, 7.86.

Ru(terpy*)(dmp)(MeOBN)(PF_6)$_2$. There were 26.7 mg of **7** (0.0251 mmol) and 232 mg of 2,6-dimethoxybenzonitrile (56 equiv, 1.42 mmol) dissolved in 15 mL of acetone. The solution was degassed and refluxed under argon for 30 min. Acetone was evaporated, and the solid was dissolved in freshly distilled dichloromethane, precipitated by adding ether, filtered, and purified by column chromatography on silica gel (eluent: acetone/water/KNO_3 700:66:12). To the collected fractions was added KPF_6, acetone was removed, and the solid was filtered, washed, and vacuum-dried. Yield: 18.1 mg of **8** (61%). Monocrystals were grown by slow vapor diffusion of diethyl ether in acetone. ^{1}H 300 MHz NMR δ (ppm) in acetone-d_6: 9.31 (s, 2H, $T_{3'5'}$); 8.94 (d, 3H, P_4 and $T_{33''}$); 8.49 (d, 1H, P_7); 8.39 (d, 1H, P_5); 8.34 (d, 1H, P_6); 8.20 (d, 1H, P_3); 8.19 (td, 2H, $T_{44''}$); 8.11 (d, 2H, T_o); 8.03 (dm, 2H, $T_{66''}$); 7.81 (t, 1H, T_p); 7.53−7.46 (4H, P_8, $T_{55''}$ and B_p); 6.65 (d, 2H, B_m, $^3J_{m-p}$ = 8.6 Hz); 3.77 (s, 6H, OMe(B)); 1.48 (s, 18H, $CH_3(^tBu)$). In the notation, B stands for the ligand 2,6-dimethoxybenzonitrile.

Ru(terpy*)(dmp)(dms)(PF_6)$_2$. There was 20.4 mg of **7** (0.0192 mmol) put under argon, a degassed mixture of 5 mL of dimethyl sulfide and 1 mL acetone were added, and the solution was irradiated under argon for 30 min. The solvents were removed under vacuum, and the complex was recrystallized overnight by slow vapor diffusion of $^iPr_2O$ in acetone in the dark. The orange crystals were isolated and washed with $^iPr_2O$ to give 10.4 mg (50%) of **9**. Monocrystals suitable for X-ray analysis were obtained by slow diffusion of $^iPr_2O$ in CH_2Cl_2 in the dark. ^{1}H 300 MHz NMR δ (ppm) in CD_2Cl_2: 8.67 (d, 1H, P_4); 8.65 (s, 2H, $T_{3'5'}$); 8.52 (d, 2H, $T_{33''}$); 8.16−8.05 (d + d + d + td, 5H, P_3 + P_5 + P_7 + $T_{44''}$); 7.92 (d, 1H, P_6); 7.82 (d, 2H, T_o); 7.74 (t, 1H, T_p); 7.69 (dd, 2H, $T_{66''}$); 7.41 (m, 2H, $T_{55''}$); 7.25 (d, 1H, P_8); 3.43 (s, 3H, $CH_3(P_2)$); 1.72 (s, 3H, $CH_3(P_9)$); 1.49 (s, 18H, tBu); 1.11 (s, 6H, $(CH_3)_2S$). ES-MS *m*/*z* (calcd): 793.3 (793.3, $[M - 2PF_6]^+$), 396.5 (396.7, $[M - 2PF_6]^{2+}$), 365.5 (365.6, $[M - 2PF_6 - (CH_3)_2S]^{2+}$). Anal. Calcd for $C_{45}H_{51}F_{12}N_5P_2Ru$: C, 49.91; H, 4.56; N, 6.47. Found: C, 49.61; H, 4.94; N, 6.36.

Ru(terpy*)(dmp)(py)(PF_6)$_2$. There was 24.2 mg of **7** (0.0228 mmol) dissolved into 2 mL of pyridine and heated at 110 °C under argon for 1 h. To the cooled solution were added saturated aqueous KPF_6 solution and water until precipitation was complete. The solid was then filtered and recovered in the absence of light with acetone. The crude product was purified on silica gel (eluent: acetone/water/sat. aq KNO_3 60:5:1) to yield 19 mg of **10** (76%). ^{1}H 300 MHz NMR δ (ppm) in acetone-d_6: 9.15 (s, 2H, T3′5′); 8.90 (m, 3H, P_4 + $T_{33''}$); 8.44 (d, 1H, P_7); 8.39 (d, 1H, P_5); 8.22−8.11 (m, 6H, P_3 + P_6 + $T_{44''}$ + $T_{66''}$); 8.02 (d, 2H, T_o); 8.00 (m, PY_o); 7.85 (tt, 1H, PY_p); 7.76 (t, 1H, T_p); 7.53 (m, 2H, $T_{55''}$); 7.44 (d, 1H, P_8); 7.27 (m, PY_m); 2.41 (s, 3H, $CH_3(P_2)$); 1.99 (s, 3H, $CH_3(P_9)$); 1.46 (s, 18H, tBu). ES-MS *m*/*z* (calcd): 955.277 (955.263, $[M - PF_6]^+$), 405.149 (405.149, $[M - 2PF_6]^{2+}$), 365.627 (365.628, $[M - 2PF_6 - py]^{2+}$). Anal. Calcd for $C_{48}H_{48}F_{12}N_6P_2Ru$: C, 52.46; H, 4.40; N, 7.64. Found: C, 52.55; H, 4.48; N, 7.68.

Acknowledgment. We would like to thank the CNRS for financial support and the European Commission for Marie Curie Postdoctoral Fellowship (ERS). S.B. acknowledges support from the Région Alsace. We thank André De Cian and Nathalie Gruber for the X-ray structures and also Johnson Matthey Inc. for a loan of $RuCl_3$.

Supporting Information Available: X-ray crystallographic files in CIF format for the structure determination of compounds **3**, **5**, **8**, and **9**. Experimental data concerning the quantum yield determinations. View of dimeric units of **3** and **8**. This material is available free of charge via the Internet at http://pubs.acs.org.

IC0491736